Journal of Alloys and Compounds 509S (2011) S782–S785

Contents lists available at ScienceDirect

Journal of Alloys and Compounds

journal homepage: www.elsevier.com/locate/jallcom

Electrochemical properties of $Ti_{45}Zr_{38-x}Ni_{17+x}$ $(0 \leq x \leq 8)$ quasicrystals produced by rapid-quenching

Akito Takasaki [a,*], Chihiro Kuroda [a], Sang-Hwa Lee [b], Jae-Yong Kim [b]

[a] Department of Engineering Science and Mechanics, Shibaura Institute of Technology, 3-7-5 Toyosu, Koto-ku, Tokyo 135-8548, Japan
[b] Department of Physics, Hanyang University, 17 Haengdang-dong, Seongdong-gu, Seoul 133-791, South Korea

ARTICLE INFO

Article history:
Received 16 July 2010
Received in revised form 28 October 2010
Accepted 8 November 2010
Available online 12 November 2010

Keywords:
Quasicrystal
Discharge capacity
Rapid-quenching
Titanium–zirconium–nickel

ABSTRACT

Discharge performances of $Ti_{45}Zr_{38-x}Ni_{17+x}$ $(0 \leq x \leq 8)$ ribbons produced by rapid-quenching were measured by a three-electrode cell at room temperature, and the effect of substitution of Ni for Zr was investigated. All the ribbons after rapid-quenching were mostly the icosahedral (i) quasicrystal phase with a negligible amount of C14 Laves phase (hcp). The discharge capacity increased with increasing amount of Ni substituted for Zr. The maximum discharge capacity achieved was about 90 mAh/g from ($Ti_{45}Zr_{30}Ni_{25}$) ribbon after substitution of Ni for Zr. The discharge performance was almost stable against the charge/discharge cycle (until 15 cycles) for all the ribbons, and the i-phase structure was also stable even after the 15th charge/discharge cycle. No metal hydride formation was observed.

1. Introduction

Because Ti–Zr–Ni icosahedral (i) quasicrystal phases, which have a new type of translational long-range order and display non-crystallographic rotational symmetry, are believed to possess a large number of tetrahedral interstitial sites in their quasilattices [1], the i-phase alloys are attractive as one of hydrogen storage materials. We have previously investigated electrochemical hydrogenation/dehydrogenation properties of $Ti_{45}Zr_{38}Ni_{17}$ amorphous and i-phase electrodes produced by mechanical alloying (MA) and subsequent annealing, and reported that the maximum discharge capacity for the i-phase electrode at room temperature was about 24 mAh/g at current density of 15 mA/g, while that for the amorphous one with identical composition was about 6 mAh/g [2]. Although the discharge capacity of the i-phase was larger than that of the amorphous, the measured discharge capacity was extremely low even for the i-phase electrode if we compare with the theoretical charge capacity (795 mAh/g for $Ti_{45}Zr_{38}Ni_{17}$ i-phase electrode) estimated from its chemical composition, suggesting that some hydrogen atoms located at the interstitial sites in the quasilattice were strongly bound with neighboring atoms. To improve the performance of the $Ti_{45}Zr_{38}Ni_{17}$ electrodes, we have recently investigated the effect of substitution of Ni for Zr or Ti on the discharge capacities of the amorphous and the i-phase electrodes produced by MA and subsequent annealing [3]. We reported that the substitution of Ni for Zr was more effective in improving the discharge capacity. The largest values were obtained for $Ti_{45}Zr_{30}Ni_{25}$, which were about 60 mAh/g for the amorphous electrode and 100 mAh/g for the i-phase electrode [3]. However, in addition to the quasicrystal, the i-phase electrodes produced by MA and subsequent annealing also contained a Ti_2Ni type crystal phase (fcc); the fraction of this phase depended on the alloy composition. Accurate measurements for the i-phase are therefore needed. In this study, we attempted to produce $Ti_{45}Zr_{38-x}Ni_{17+x}$ $(0 \leq x \leq 8)$ ribbons, which substituted Ni for Zr from ($Ti_{45}Zr_{38}Ni_{17}$) standard composition, by rapid-quenching, and we investigated microstructures of the ribbons, measured their electrochemical properties, and discussed the effect of substitution of Ni for Zr on the discharge performance of the electrodes produced by rapid-quenching.

2. Experimental procedures

Pieces of Ti, Zr, and Ni (purities of higher than 99.9%) with chemical compositions of $Ti_{45}Zr_{38-x}Ni_{17+x}$ $(0 \leq x \leq 8)$ were arc-melted in an argon atmosphere on a Cu hearth which was cooled by water. To minimize the oxygen contamination, the sample chamber was evacuated to the level of 10^{-5} Pa and back filled with a high-purity argon gas several times. The ingots were melted and then turned over at least three times to homogenize the chemical compositions. The obtained ingots were then crushed and subsequently rapid-quenched on a stainless-steel wheel that rotated at 1000–5000 rpm in a vacuum. The ribbons after rapid-quenching were 30–50 μm thick, 2–5 cm long, and 2 mm wide.

The ribbons were gently milled (by a mortar and pestle), and electrochemical measurements were performed in a three-electrode cell. Mixtures containing 25 wt% active materials ($Ti_{45}Zr_{38-x}Ni_{17+x}$ $(0 \leq x \leq 8)$) and 75 wt% nickel powder (99.9% pure) were compacted at a pressure of 10 MPa, and used as working electrodes. The counter electrode and reference electrode were $Ni(OH)_2$/NiOOH and Hg/HgO, respectively. The counter electrode was prepared using commer-

* Corresponding author. Tel.: +81 3 5859 8059; fax: +81 3 5859 8001.
E-mail address: takasaki@sic.shibaura-it.ac.jp (A. Takasaki).

0925-8388/$ – see front matter © 2010 Elsevier B.V. All rights reserved.
doi:10.1016/j.jallcom.2010.11.042

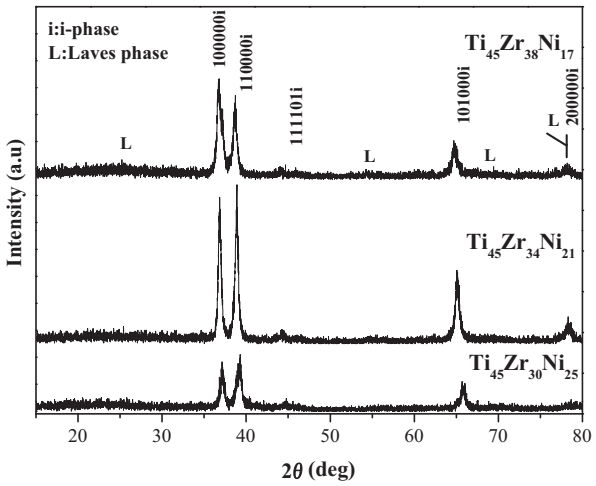

Fig. 1. X-ray diffraction patterns for Ti–Zr–Ni electrodes produced by rapid-quenching.

cial $Ni(OH)_2$ powder of 99% purity. Nickel hydroxide powders were mixed with elemental Ni powder (with a mass ratio of 1:15), pressed and compacted at a pressure of 10 MPa, and then annealed at 473 K for 12 h. The mass of the counter electrode was determined to provide an electrochemical capacity of twice the theoretical capacity of the working electrode. The cell electrolyte was a 6 M KOH aqueous solution. Charge/discharge tests were carried out using an HJ-201B (Hokuto Denko Co Ltd.), which is a galvanostatic system. The first charging step (hydrogenation) was carried out for 14 h, while each subsequent charging step lasted for 2 h. The current density was maintained at 70 mA/g for all charging (hydrogenation) steps. For discharging (dehydrogenation) steps, a cutoff potential was set at −0.6 V vs. the Hg/HgO electrode. During discharging, the current density was set at 15 mA/g. After charging and discharging, the electrodes were relaxed for 10 min. The charge/discharge tests were performed at room temperature. X-ray diffraction (XRD) measurements were performed to identify the microstructures before and after charging/discharging steps, using a Rigaku Ultima IV with Cu-Kα radiation at 45 kV and 40 mA.

3. Results and discussion

Fig. 1 shows XRD patterns for $Ti_{45}Zr_{38-x}Ni_{17+x}$ $(0 \le x \le 8)$ ribbons produced by rapid-quenching. The microstructure of all ribbon was mostly the i-phase with a negligible amount of C14 Laves phase (hcp). The XRD peaks corresponding to the i-phase were indexed using a six-index scheme proposed by Bancel et al. [4]. The two main XRD peaks corresponding to the i-phase ((1 0 0 0 0 0) and (1 1 0 0 0 0)) became stronger and sharper with decreasing amounts of Zr from 38 at% to 34 at% (or increasing amounts of Ni from 17 at% to 21 at%), but became weaker and broader with further substitution of Ni for Zr. The best coherence length (or quality) of the i-phase was obtained from ($Ti_{45}Zr_{34}Ni_{21}$). We have previously reported that an amorphous phase produced after MA transformed into the i-phase together with a Ti_2Ni-type crystal phase (fcc), whose amount was dependent on their chemical composition, after annealing. However, the Ti_2Ni-type phase was not detected in the present samples after rapid-quenching. Therefore, we can eliminate the effect of the Ti_2Ni-type phase from the total discharge capacity.

Fig. 2(a) and (b) shows discharge curves obtained for the first 15 cycles for $Ti_{45}Zr_{38}Ni_{17}$ and $Ti_{45}Zr_{30}Ni_{25}$ i-phase electrodes produced by rapid-quenching respectively. Although the discharge curves (potential) for $Ti_{45}Zr_{38}Ni_{17}$ rapidly decreased, that for $Ti_{45}Zr_{30}Ni_{25}$ moderately decreased until the discharge capacity of about 40 mAh/g. The maximum discharge capacities for the $Ti_{45}Zr_{38-x}Ni_{17+x}$ $(0 \le x \le 8)$ electrodes as a function of charge/discharge cycle are shown in Fig. 3. The achieved maximum discharge capacities for all ribbon were almost stable until the 15th cycle, although those for $Ti_{45}Zr_{30}Ni_{25}$ fluctuated slightly

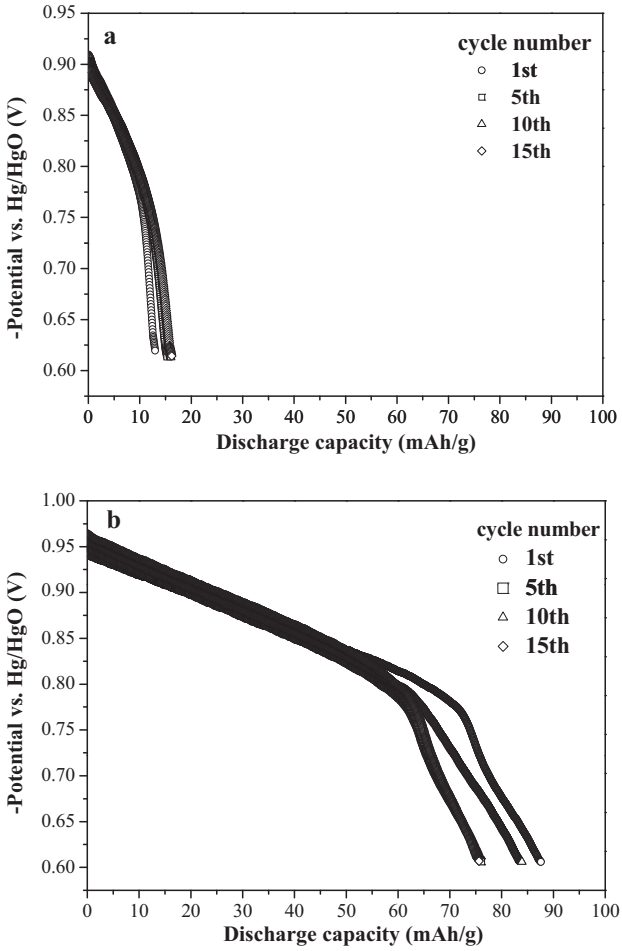

Fig. 2. Discharge curves obtained for the first 15 cycles for (a) $Ti_{45}Zr_{38}Ni_{17}$ and (b) $Ti_{45}Zr_{30}Ni_{25}$ i-phase electrodes.

at a beginning of the cycling. The maximum discharge capacity for $Ti_{45}Zr_{38}Ni_{17}$ was about 20 mAh/g, which is very similar to the identical i-phase electrode produced by MA and subsequent annealing (24 mAh/g) we have previously reported [2]. The discharge capacity increased with increasing amounts of Ni substitution for Zr. Thus, the substitution of Ni for Zr is effective to improve the discharge capacity. The highest discharge capacity obtained was about

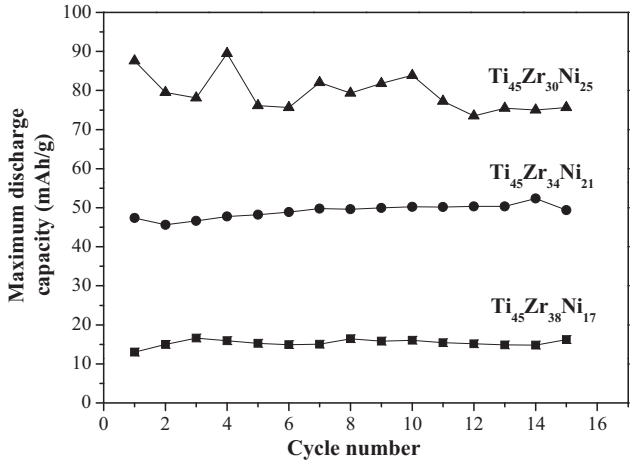

Fig. 3. The maximum discharge capacities for Ti–Zr–Ni electrodes as a function of charge/discharge cycle.

Table 1
Theoretical charge capacities and measured discharge capacities for Ti–Zr–Ni i-phase electrode produced by rapid-quenching.

Composition	Theoretical charge capacity [mAh/g]	Measured maximum discharge capacity [mAh/g]
$Ti_{45}Zr_{38}Ni_{17}$	696.47	16.58
$Ti_{45}Zr_{34}Ni_{21}$	623.70	52.33
$Ti_{45}Zr_{30}Ni_{25}$	598.53	87.58

90 mAh/g from ($Ti_{45}Zr_{30}Ni_{25}$) electrode after substitution of Ni for Zr, which is also similar to the identical i-phase electrode produced by MA and subsequent annealing (about 100 mAh/g) we reported previously [3]. Because the present results are similar to those produced by MA and subsequent annealing, it is suggested that the Ti_2Ni-type crystal phase, generally appeared with the i-phase after MA and subsequent annealing, would not strongly affect the discharge capacity of the i-phase electrodes. Although the discharge capacities for the electrodes produced by MA and subsequent annealing were relatively low early in the charge/discharge cycling due to a thin oxide layer covering the electrodes [3], those produced by rapid-quenching were almost constant from the beginning of the cycle, which means activation treatment are not required for the electrodes produced by rapid-quenching. Liu et al. reported discharge capacities for several quaternary Ti-based i-phase electrodes, which were 76 mAh/g for a $Ti_{45}Zr_{38}Ni_{17}Cu_3$ [5], 109 mAh/g for a $Ti_{45}Zr_{30}Ni_{25}La_3$ [6], and 148 mAh/g for a $Ti_{45}Zr_{35}Ni_{13}Pd_7$ [7]. They also reported that adequate ball-milling could increase the discharge capacity of a $Ti_{45}Zr_{38}Ni_{17}Cu_3$ i-phase electrode with 20 mass% Ni from 89 to 192 mAh/g, although the quality of the i-phase worsened [8]. They have recently reported that discharge capacities of a melt-spun Ti–Zr–Ni–La decreased from 109 mAh/g to 99 mAh/g with increasing La concentration [9]. Their discharge capacities are very comparable to our results. Table 1 summarizes the theoretical charge capacities, which were estimated from the maximum number of hydrogen atoms present in the unit mass of the sample and Faraday's constant, and achieved discharge capacities for the i-phase electrode produced by rapid-quenching. The achieved discharge capacity for $Ti_{45}Zr_{30}Ni_{25}$ was still low, when compared with the theoretical charge capacity (599 mAh/g). It is suggested that most hydrogen atoms that entered the i-phase structure (probably the tetrahedral interstitial sites) are strongly bound with neighboring atoms in the quasilattice and cannot be removed electrochemically.

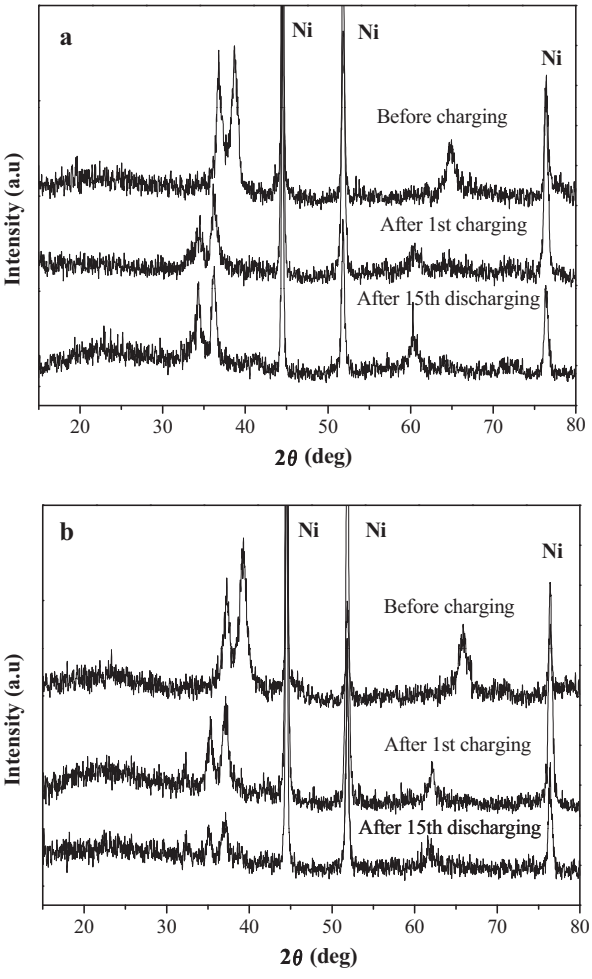

Fig. 4. X-ray diffraction patterns for (a) $Ti_{45}Zr_{38}Ni_{17}$ and (b) $Ti_{45}Zr_{30}Ni_{25}$ before charging and after charging/discharging cycling.

Fig. 4(a) and (b) shows XRD patterns for $Ti_{45}Zr_{38}Ni_{17}$ and $Ti_{45}Zr_{30}Ni_{25}$, respectively, before charging and after charging/discharging cycling. The strong XRD peaks were due to Ni because the electrodes were mixtures of the gently milled i-phase ribbons and Ni powders as mentioned earlier. For both samples, the XRD peaks corresponding to the i-phase shifted to lower angles after the 1st charging, and shifted back slightly after the 15th discharging without formation of metal hydride like TiH_2, demonstrating the high stability of the i-phase structure during electrochemical charging and discharging. In any i-phase electrode, the quasilattice constant [10] increased about 5.5–5.9% (which correspond to about 1.4–1.5 of H/M) after the 1st charging step, indicating the expansion of the quasilattice after hydrogenation. The quasilattice constants for both electrodes after the 15th discharging step never returned to their values before the first charging step, indicating that most of the hydrogen entering the quasilattice structure during charging could not be removed.

4. Conclusions

Microstructures and discharge performance for $Ti_{45}Zr_{38-x}Ni_{17+x}$ ($0 \le x \le 8$) ribbons produced by rapid-quenching were investigated. Although the coherence length of the i-phase depended on the amount of substitution of Ni for Zr, all the ribbons were the i-phase with a negligible amount of C14 Laves phase (hcp). The i-phase was stable without forming any metal hydride against charging/discharging cycle until the 15th cycle. The maximum discharge capacity achieved was about 90 mAh/g for ($Ti_{45}Zr_{30}Ni_{25}$) i-phase electrode after substitution of Ni for Zr, but was much lower than the theoretical charge capacity (about 599 mAh/g). It is suggested that most hydrogen atoms that entered the i-phase structure are strongly bound with neighboring atoms in the quasilattice and cannot be removed electrochemically. Further modification of the i-phase electrodes is needed for the actual battery applications.

Acknowledgements

This research was partially supported by the European Commission (project Dev-BIOSOFC, FP6-042436, MTKD-CT-2006-042436).

References

[1] P.C. Gibbons, K.F. Kelton, in: Z.M. Stadnik (Ed.), Physical Properties of Quasicrystals, Springer, 1999, p. 403.
[2] A. Takasaki, W. Zając, T. Okuyama, J.S. Szmyd, J. Electrochem. Soc. 156 (2009) A521.
[3] A. Takasaki, T. Okuyama, J. Szmyd, J. Mater. Res. 25 (2010) 1575.

[4] P.A. Bancel, P.A. Meiney, P.W. Stephens, A.I. Goldman, P.M. Horn, Phys. Rev. Lett. 54 (1985) 2422.
[5] B. Liu, Y. Wu, L. Wang, J. Power Sources 159 (2006) 1458.
[6] B. Liu, J. Liu, G. Mi, Z. Zhang, Y. Wu, L. Wang, J. Alloys Compd. 475 (2009) 881.
[7] B. Liu, Y. Zhang, G. Mi, Z. Zhang, L. Wang, Int. J. Hydrogen Energy 34 (2009) 6925.
[8] B. Liu, Y. Wu, L. Wang, J. Power Sources 162 (2006) 713.
[9] B. Liu, J. Liu, G. Mi, Z. Zhang, Y. Wu, L. Wang, J. Alloys Compd. 475 (2009) 881–884.
[10] V. Elser, Phys. Rev. B32 (1985) 4892.